Journal Pre-proof

The effect of metal precursor on copper phase dispersion and nanoparticle formation for the catalytic transformations of furfural

Mohammed J. Islam, Marta GranollersMesa, Amin Osatiashtiani, Martin J. Taylor, Jinesh C. Manayil, Christopher M.A. Parlett, Mark A. Isaacs, Georgios Kyriakou

PII: S0926-3373(20)30477-X

DOI: https://doi.org/10.1016/j.apcatb.2020.119062

Reference: APCATB 119062

To appear in: *Applied Catalysis B: Environmental*

Received Date: 15 February 2020

Revised Date: 22 April 2020

Accepted Date: 23 April 2020

Please cite this article as: Islam MJ, GranollersMesa M, Osatiashtiani A, Taylor MJ, Manayil JC, Parlett CMA, Isaacs MA, Kyriakou G, The effect of metal precursor on copper phase dispersion and nanoparticle formation for the catalytic transformations of furfural, *Applied Catalysis B: Environmental* (2020), doi: https://doi.org/10.1016/j.apcatb.2020.119062

The effect of metal precursor on copper phase dispersion and nanoparticle formation for the catalytic transformations of furfural

Mohammed J. Islam[a], Marta Granollers Mesa[a], Amin Osatiashtiani[a], Martin J. Taylor[b], Jinesh C. Manayil[a], Christopher M. A. Parlett[c,d,e], Mark A. Isaacs[f,g], and Georgios Kyriakou[h]*

[a] Energy & Bioproducts Research Institute (EBRI), Aston University, Aston Triangle, Birmingham, B4 7ET, United Kingdom

[b] Energy and Environment Institute, University of Hull, Cottingham Road, Hull, HU6 7RX, United Kingdom

[c] School of Chemical Engineering and Analytical Science, University of Manchester, Manchester, M1 3AL, United Kingdom

[d] University of Manchester at Harwell, Diamond Light Source, Harwell Campus, Didcot, OX11 0DE, United Kingdom

[e] Spectroscopy village, Diamond Light Source, Harwell Science and Innovation Campus, Didcot, OX11 0DE, United Kingdom

[f] Department of Chemistry, University College London, London, WC1H 0AJ, United Kingdom

[g] HarwellXPS, Research Complex at Harwell, Rutherford Appleton Labs, Didcot, OX11 0FA, United Kingdom

[h] Department of Chemical Engineering, University of Patras, Caratheodory 1, Patras GR 265 04, Greece

*Corresponding author, E-mail address: kyriakg@upatras.gr (G. Kyriakou)

Graphical abstract

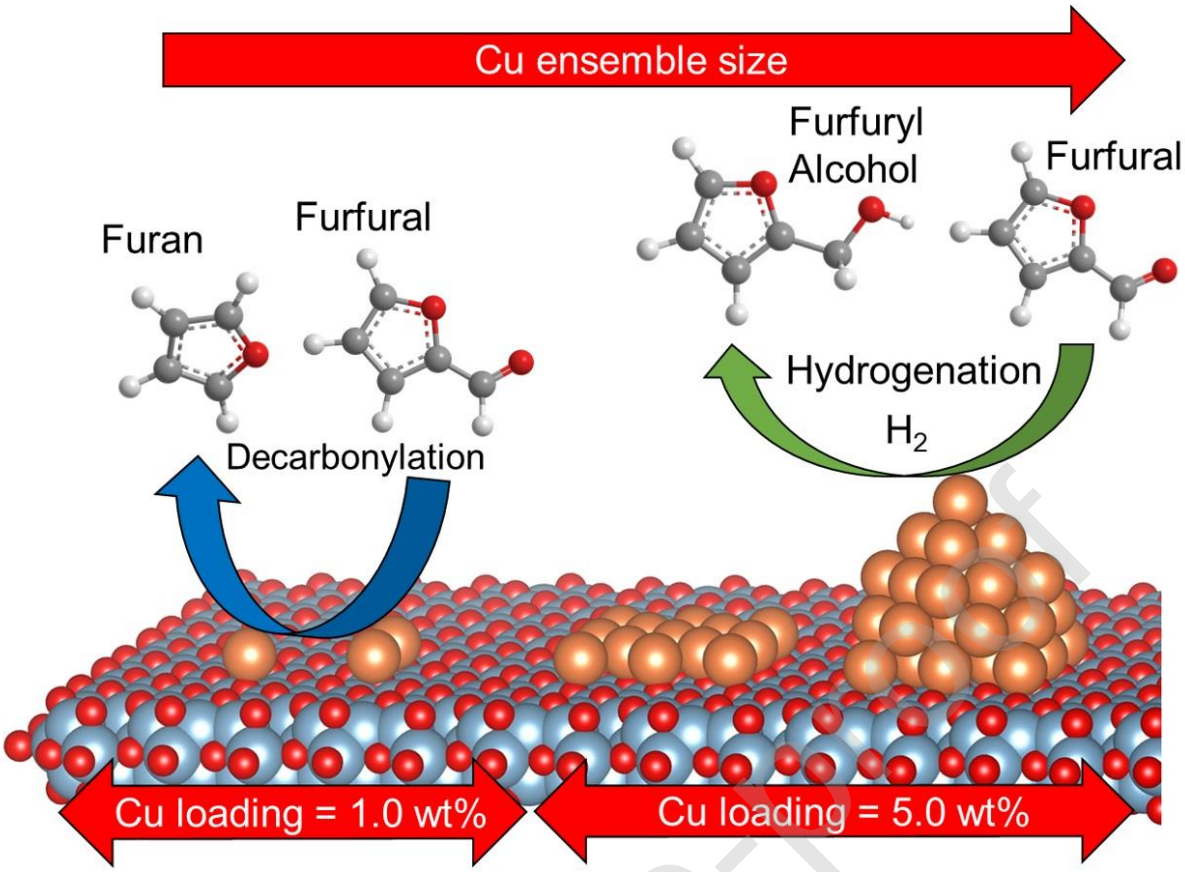

Highlights

- Highly dispersed Cu on Al_2O_3 catalyses the selective furfural hydrogenation.
- Cu metal precursor selection is crucial for furfural hydrogenation.
- Atomic and dimeric Cu species favour furfural decarbonylation reactions.
- Sulphur impurities selectively promote the formation of biproducts.

Abstract

The formation of copper-based catalysts ranging from nanoparticles to isolated and dimeric Cu species supported on nanophased alumina is reported and utilised for the catalytic liquid-phase hydrogenation of furfural. The materials were synthesised via wet impregnation using various copper precursors (nitrate, acetate and sulphate) at two different loadings. A high Cu loading (5 wt%) led to the formation of well-defined nanoparticles, while a lower loading (1

wt%) generated a highly dispersed phase consisting mostly of atomic and dimeric Cu species dispersed on Al_2O_3. The catalytic reaction was found to be structure sensitive, promoting decarbonylation reactions with low Cu loading. Copper sulphate derived catalysts were found to severely decrease furfuryl alcohol selectivity from 94.6% to 0.8%, promoting the formation of side reactions. The sulphur-free catalysts represent a greener and more sustainable alternative to the toxic catalysts currently used in industry, operating at milder conditions of 50 °C and 1.5 bar H_2.

Keywords

Copper; Furfural; Nanoparticle, Hydrogenation; Single atom catalysts

1 Introduction

The ever-increasing demand for 'drop-in' fuels, fuel additives, and fine chemicals is spurred on by the perpetual growth in global demand. The use of bio-renewable feedstocks as alternative fuels has become an attractive, green and carbon-neutral option to move away from fossil fuel reserves [1, 2]. However, this switch has a detrimental impact on the chemical industry, since the majority of fuels and chemicals are derived from non-renewable petroleum and natural gas resources [3]. As a result, the development of the biorefinery has become the cornerstone for the production of sustainable fuels, chemicals and energy. This has motivated the development of novel catalytic processes capable of selectively converting lignocellulosic biomass waste-derived bio-oil into value-added chemicals.

Among such biomass-derived compounds are furfural and its derivatives, which have been identified as one of the top 30 biomass-derived platform chemicals by the U.S. Department of energy [4]. The process of furfural production, primarily based on the acid-catalysed transformation of xylose from hemicellulose [5], was commercialised by the Quaker Oat Company in 1921 [6]. Furfural is used to synthesize high volume products such as polyols, which can be used directly as monomer precursors for the polyester industry, or in the production of other polymers such as polyurethanes and polyamides [3, 7]. However, the majority of furfural consumption (~62%) is used to produce furfuryl alcohol through a selective hydrogenation pathway [8], a transient molecule that can be used to synthesise ascorbic acid, lubricants, anti-corrosive coatings, perfumes and flavourings and, primarily for furan based resins [9, 10]. For the past 90 years, current industrial processes for the selective transformation of furfural to furfuryl alcohol utilise copper chromate catalysts [9, 11-13] operating at conditions as high as 200 °C, and pressures up to 30 bar [3]. A variety of methods exist for the

production of copper chromate catalysts, including co-impregnation, co-precipitation and solid-state synthesis which often time-consuming or ultimately use environmentally harmful materials [14]. While such catalysts demonstrate good activity and selectivity towards furfuryl alcohol, due to their poor stability over time, chromic oxide is produced which is highly toxic and causes severe environmental problems. On an industrial scale, this leads to large-scale disposal problems and contamination downstream. Consequently, there is a drive for energy-efficient and environmentally friendly alternative processes and materials, which accommodate milder temperature and pressure constraints.

A variety of alternative metal catalysts have been investigated previously for both the gas and liquid phase hydrogenation of furfural, such as Ir, Pd, Pt, Ru, Ni, Co and Cu [15-20]. Such investigations have found that the chemical transformation of furfural on transition metal catalysts is dependent on the affinity of reactants for the metal, both in terms of hydrogen-metal and furfural-metal interaction [4, 21]. Taylor et al. [3] studied the effect of support on the Pt catalysed liquid phase hydrogenation of furfural to furfuryl alcohol. The authors studied a variety of supports of different acidity, surface area, and crystallinity. Despite their major physicochemical differences, supports like MgO, CeO_2 and γ-Al_2O_3 appeared to perform very well in the selective hydrogenation of furfural to furfuryl alcohol. Although, there was no evidence of strong metal-support interactions the support selection appeared to be important to achieve a good dispersion of the metal. In this case, crystalline nano-Al_2O_3 was used which allows the active Cu phase to be more accessible to the substrate as compared, for instance with standard porous aluminas which often suffer from mass transfer problems as well as the blocking of pores and deterioration of the surface area at high temperatures/prolonged use. Furfural is a functionalised molecule that can bind to the catalyst's surface in various bonding motifs, which can strongly influence its reactivity [22]. The most widely accepted mechanism for Pt group metals catalysts comes from density functional theory (DFT) calculations. It has been suggested that furfural prefers the η^2(C, O)-aldehyde conformation (an end on motif), where both O and C atoms are bound to the metallic surface [4, 23, 24]. However, at higher temperatures the preferred binding mode changes to a η^1(C)-acyl conformation (planar to the surface), which thermodynamically favours the decarboxylation of furfural to produce furan [24, 25]. In contrast, DFT calculations for Cu surfaces suggest that furfural prefers the η^1(O)-aldehyde binding mode [21, 25], where the carbonyl functional group is directly attached to the surface via oxygen's lone pair of electrons. This bonding mode is preferred due to the weak affinity that the Cu metal surface has for C=C bonds and as a result, favours the hydrogenation

of the C=O bond [26]. The enhanced selectivity due to the η^1(O)-aldehyde binding mode is demonstrated by Lesiak et al. [17] where 100% furfuryl alcohol selectivity is reported with a monometallic Cu/Al_2O_3 at 90 °C. It is also reported by Srivastava et al. [27] that while at mild reaction temperatures Cu based catalysts prefer furfuryl alcohol formation, at thermally intensive conditions (170 °C) hydrogenolysis and polymerisation of furfuryl alcohol becomes favoured.

Sulphur has been widely used in hydrodeoxygenation reactions for Mo, Ni, Co-based catalysts [28, 29]. It is also reported that sulphided sites in sulphided NiMo based catalysts can promote hydrogen transfer for hydrogenation reactions [30] in conjunction with aldol condensation reactions [31, 32] during the hydrotreatment of aldehydes. However, these sulphided catalysts can suffer from leaching, leading to a decline in activity and sulphur contamination of the products [33]. But how sulphur interacts with a copper surface and its influence on catalytic hydrogenation reactions is not yet fully understood. Previously, the modification of copper surfaces with sulphur was also thoroughly studied for the hydrogenation of crotonaldehyde, both on single crystals and dispersed catalysts [34-38]. Lambert and co-workers [35, 39] found that sulphur atoms activate the copper surface towards the chemoselective hydrogenation of crotonaldehyde. The presence of S adatoms electronically perturbs and strongly tilt the reactant favouring C=O hydrogenation over C=C hydrogenation. Their observations also supported earlier work done by Hutchings et al. [34, 37, 38], who reported the introduction of sulphur to Cu/Al_2O_3 catalysts for crotyl alcohol production, here acting as a promoter under atmospheric conditions. Conversely, May et al. [40] reported that sulphur addition can act as a poison, since it changes the electron characteristics of the surface, such as the work function, altering the metal-metal distances in the top-most atomic row.

This work investigates the effect of metal precursors in the synthesis of Cu/Al_2O_3 catalysts via a simple wet impregnation method. The synthesis was investigated in two distinct Cu loadings the first one leading to the formation of metal nanoparticles and the second one leading to the formation of a highly dispersed Cu phase consisting mostly of single atoms and dimers on the alumina surface. The role of sulphur impurities on the catalyst surface in the selective hydrogenation of furfural was also investigated by comparing Cu/Al_2O_3 catalysts prepared using two sulphur-free precursors and one sulphur-containing precursor. Furthermore, by utilising the mechanism by which Cu binds to the alumina's surface prior to the catalytically necessary reduction, initially forming rows of copper ions at low coverage and as the

loading/calcination temperature increases paracrystalline and finally crystalline CuO [41], the structure sensitivity of the reaction was explored.

2 Experimental

2.1 Catalyst synthesis

The alumina-supported monometallic copper catalysts were synthesised via a wet impregnation method utilising $Cu(NO_3)_2$ (Sigma-Aldrich, 99.999%), $Cu(CO_2CH_3)_2$ (Sigma-Aldrich, 98%) and $CuSO_4.5H_2O$ (Sigma-Aldrich, ≥98.0%). The Cu precursors were dissolved in distilled water (5 mL), then introduced to the nanophase Al_2O_3 support (Alfa Aesar, NanoArc, 99.5%, 32-40 $m^2\ g^{-1}$) consisting of 70 wt% δ-phase and 30 wt% γ-phase, generating materials with a nominal Cu loading of 1 wt% and 5 wt%. The mixtures were stirred for 2 h at ambient temperature and pressure conditions followed by drying overnight at 100 °C. The obtained solid was then finely ground and calcined for 4 h in air at 500 °C. The synthesised catalysts were denoted as Cu (N), Cu (A) and Cu (S) for the materials synthesised from copper nitrate, copper acetate and copper sulphate precursors, respectively.

2.2 Material characterisation

Scanning Transmission Electron Micrographs (STEM) were acquired on a Cs aberration-corrected JEOL 2100F microscope operating at 200 kV. Images were acquired using a Gatan Ultrascan 4000 digital camera. Samples were dispersed in methanol using sonication and deposited on 300-mesh carbon-supported copper grids and dried at 60 °C. ImageJ 1.52a software was used for image analysis.

Elemental contents were determined by inductively coupled plasma optical emission spectroscopy (ICP-OES) using a Thermo Scientific iCAP 7400 Duo. The samples were prepared by adding ~10 mg of the catalyst to 2 mL HCl (VWR Chemicals, 37%) and 5 mL H_2SO_4 (Fisher Scientific, >95%). The mixture was then heated to 280 °C for 1 h to ensure the complete dissolution of aluminium oxide and then cooled to room temperature, this was followed by adding 3 mL of HNO_3 (VWR Chemicals, 68%) to ensure that the copper is fully

dissolved. Digestates were made up to 10 mL with deionised water to replace any evaporation loses. Finally, 1 mL of digestant was diluted in a 1:9 ratio with deionised water before analysis.

BET surface areas were determined via N_2 physisorption using a Quantachrome Nova 4000 instrument. The samples were degassed at 120 °C for 2 h before analysis at -196 °C. Surface areas were calculated using the Brunauer–Emmett–Teller (BET) method over the pressure range of P/P_0 = 0.03– 0.18, where a linear relationship was maintained.

X-ray photoelectron spectroscopy (XPS) and X-ray excited Auger electron spectroscopy (XAES) measurements were conducted on a Kratos AXIS Supra spectrometer equipped with a charge neutraliser and monochromated Al Kα excitation source (1486.7 eV), CasaXPS was used for subsequent data analysis. Photoelectron energies were referenced to adventitious carbon at 284.8 eV. The modified auger parameter α' was defined as the sum of the photoelectron binding energy and the auger electron kinetic energy [42]. The extra-atomic relaxation energy was defined as half the change in the modified auger parameter compared to bulk Cu [43]. Copper metal dispersion and particle sizes were estimated using a method reported previously [44-46] (see supplementary information, Table S1).

Powder X-ray Diffraction (PXRD) measurements were performed using a Bruker D8 Advance diffractometer equipped with a Lynxeye PSD detector and with Cu $K\alpha_{1,2}$ radiation (40 kV and 40 mA, 0.02mm Ni K_β absorber, 10−80° 2θ range, a step scan of 0.02° 2θ at 1 s per step). In-situ XRD measurements were conducted in an Anton-Paar XRK-900 reaction chamber in the parallel beam geometry using a Göbel mirror and 2.5° Soller slits. Diffractograms were then collected with a step scan of 0.02° 2θ and 2s per step in a flowing 20% H_2/80% He atmosphere. Whole pattern powder modelling (WPPM) [47-49] was used to calculate the arithmetic mean domain size of the Cu nanoparticles. The Caglioti et al. relationship [50] was used to estimate the instrumental contribution by modelling the peak profiles from the NIST SRM 1976b corundum standard. The slight gaussian micro-strain broadening arising from the SRM 1976b [51] was assumed negligible compared to the broadening from the nanosized copper phase. The background was created using a combination of a Chebyshev polynomial and an exponential decay. The crystalline domains were assumed to be spherical and distributed according to a log-normal size distribution. The volume-weighted crystallite size was estimated with the integral breadth method (see supplementary information).

Finally, X-ray Absorption spectra were collected at B18 XAS beamline at Diamond Light Source, United Kingdom. A double-crystal Si(111) monochromator was used to scan the X-

ray energies from -200 to 800 eV relative to the Cu K-edge (8979 eV). Following ex-situ reduction in H_2 at 300°C, the XAS measurement was conducted in transmission mode with 3 repeats; the data were aligned and averaged for further XANES and EXAFS analysis using Athena and Artemis software packages [52].

2.3 Catalytic testing

In-situ reduction and catalytic reactions were performed in a H.E.L DigiCAT high-pressure reactor system operating 3x 50 mL stainless steel autoclaves. The reactors were charged with approximately 30 mg of the catalyst, which was heated under flowing H_2 to 300 °C at 5 °C min^{-1} and held for 0.5 h. After cooling to room temperature under flowing H_2, the autoclaves were purged with He and then sealed to prevent the oxidation of the catalyst. While He was flowing, 10 mL of the reaction mixture consisting of MeOH (Fisher Scientific, HPLC grade), furfural (0.02 M, Sigma Aldrich, 99%) and the internal standard decane (0.02 M, Sigma Aldrich, 99%), was injected into each reactor. The mixtures were degassed for 10 min in flowing He before pressurising with H_2 (BOC, 99.995%). The reactors were then heated to 50 °C and stirred at 600 RPM via a magnetic stirrer. The reaction was carried out for 7 h before being cooled and depressurised to atmospheric pressure. Aliquots of the reaction mixture (0.2 mL) were taken and analysed offline without further dilution using a Bruker Scion 456 GC-FID using a Zebron ZB-5 (5%-phenyl-95%-dimethylpolysiloxane) capillary column. The concentration of the products was determined through the normalisation of the individual peak areas with the internal standard, as well as the use of 5-point calibration standards of the pure compounds. All peaks in the chromatograph were identified via GC-MS where erroneous peaks from impurities in the solvent were identified and discarded by comparing. Errors in the reported conversions/selectivity were estimated to have a relative standard deviation of ±5% and carbon mass balances of ~97%.

3 Results and discussions

3.1 Characterisation of the catalysts

3.1.1 Elemental, Surface Area and Particle Size Analysis

Table 1 shows the elemental analysis and the surface area measurements of the catalysts after calcination and reduction. The loading of the catalysts was found to be close to the nominal loading while the slight differences in loading between the precursors is due to differences in the thermal stability and reducibility of the precursors [53-55]. A type II isotherm was observed (Fig. S1) for the reduced catalytic materials and the bare support after calcination

and reduction showing that the materials are non-porous/macro-porous. The surface area measurements of the catalytic materials were found to be very close to the surface area of the bare support.

Table 1 Bulk elemental analysis, surface area measurements, Cu crystallite and Cu particle size analysis. Catalysts synthesised using copper nitrate, copper acetate and copper sulphate pentahydrate were denoted (N), (A) and (S), respectively.

Catalyst	Nominal Cu loading (wt%)	Actual Cu loading[a] (wt%)	Surface area[b] (m^2g^{-1})	Cu crystallite size[c] (nm)	Cu crystallite size[d] (nm)	Cu particle size[e] (nm)
Cu/Al_2O_3 (N)	1.0	0.83 ± 0.04	35.9 ± 1.8	-	-	-
Cu/Al_2O_3 (A)	1.0	0.91 ± 0.05	35.0 ± 1.8	-	-	-
Cu/Al_2O_3 (S)	1.0	0.66 ± 0.08	38.8 ± 1.9	-	-	-
Cu/Al_2O_3 (N)	5.0	4.22 ± 0.32	33.5 ± 1.7	19.6 ± 4.1	13.2 ± 9.5	3.9 ± 1.9
Cu/Al_2O_3 (A)	5.0	4.56 ± 0.36	33.3 ± 1.7	19.7 ± 4.3	13.0 ± 9.4	6.8 ± 5.5
Cu/Al_2O_3 (S)	5.0	4.22 ± 0.31	29.7 ± 1.5	24.7 ± 2.8	18.7 ± 12.9	12.8 ± 9.3
Al_2O_3	-	-	38.2 ± 1.9	-	-	-

[a] Determined by ICP-OES, [b] BET surface area from N_2 porosimetry, [c]Integral breath method via XRD, [d] WPPM via XRD, [e] STEM

3.1.2 Powder X-ray Diffraction (PXRD)

Fig. 1 shows ex-situ PXRD results from all copper catalysts used in this study after reduction at 300 °C for 0.5 h. The diffractograms show broad but discernible reflections characteristic of nano-crystalline γ-Al_2O_3 (JCPDS card No. 29-0063) and δ-Al_2O_3 (JCPDS card No. 46-1215), as well as a small impurity arising from the θ-Al_2O_3 phase (JCPDS card No. 11-0517). A qualitative examination of the diffractograms shows that the nano-crystalline alumina's long-range crystal structure appears to be unchanged in all six catalysts, suggesting that the presence of the copper phase onto the alumina did not significantly impact the overall morphology of the support. In the case of the 5.0 wt% Cu catalysts, they exhibited a sharp diffraction peak at 43.4°and 50.5° which corresponds to the (111) and (200) reflections of metallic FCC Cu. This suggests that the Cu nanophase was predominately metallic after the ex-situ reduction (diffraction peaks indicative of CuO and Cu_2O at 35.5° and 42.7° could not be resolved) [56]. Interestingly, Cu diffraction peaks were not detected for the 1.0 wt% Cu samples, which, in agreement with the STEM data, show that the Cu phase is highly dispersed leading to very broad diffraction reflections.

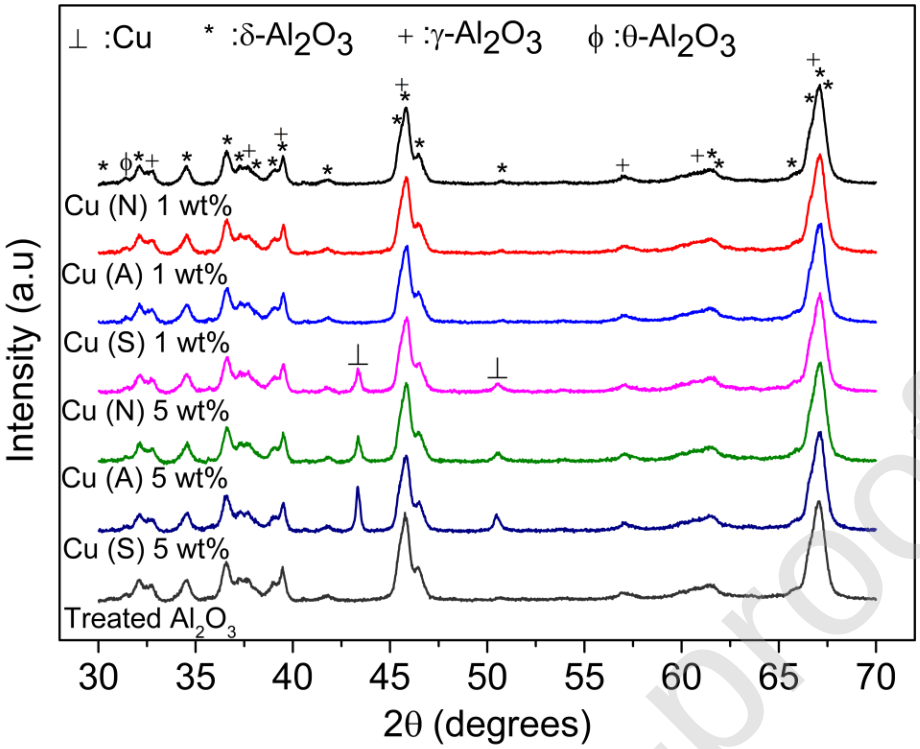

Fig. 1 PXRD patterns of reduced ex-situ Cu/Al_2O_3 catalysts synthesised from their respective copper nitrate (N), copper acetate (A) and copper sulphate (S) precursors at loadings of 5.0 wt% and 1.0 wt%.

3.1.3 Scanning Transmission Electron Microscopy (STEM)

Examination of the 1.0 wt% Cu/Al_2O_3 catalysts with STEM was not able to determine the presence of any Cu regions. This is most likely due to a combination of the low Z-contrasts between the Cu and Al entities of the catalyst and the presence of highly dispersed Cu species embedded into the Al_2O_3 which could not be resolved. The EXAFS data, discussed later, suggest that the Cu most likely exists as single atoms on the surface of the Al_2O_3 support. Contrary to this, the STEM images of the 5.0 wt% catalysts after ex-situ reduction (Fig. 2a-2e) show clearly the presence of Cu particles. Interestingly, the mean particle sizes (Table 1) for the 5.0 wt% Cu/Al_2O_3 (N) and (A) appears to be similar when calculated via PXRD (by both the integral breath and the WPPM methods). However, there is a clear deviation between the PXRD calculated and the STEM measured particle sizes of the two catalysts due to the low Z-contrast between Cu and the alumina support and the difficultly in the identification of small species: overestimating average particle size. The STEM and PXRD data for the 5 wt% Cu/Al_2O_3 catalysts indicate that part of the copper phase is dispersed into the Al_2O_3 without exhibiting a consistent geometric structure. This is attributed to the unusual mechanism in which the Cu^{2+} species are bonded to the alumina's surface; whereby the Cu^{2+} species (from

CuO) after calcination are coordinated as rows of copper ions in a tetrahedral/octahedral symmetry via alumina's oxygen atoms, extending alumina's oxide network [41, 57]. Consequently, this can give rise to isolated or paracrystalline CuO phase on the Al_2O_3 surface which is observed by an estimated 100% Cu dispersion of the calcined 1.0 wt% catalysts in Table S1. In the case of higher Cu loadings, like the 5.0 wt% Cu/Al_2O_3 (N) and (A), supporting our Cu dispersion values Marion et al. [57] suggest that by increasing the Cu loading, the Al_2O_3 surface becomes oversaturated and the tetrahedral/octahedral Cu species begin to sinter into particles from a layered structure during calcination. After reduction, the Cu dispersion appeared to decrease which is thought to be due to the strong Cu-O links to the support breaking down, allowing Cu atoms to be more mobile resulting in the formation of layers and particles. The measured lattice spacing of such layered structures after being reduced shown in Fig. 2b was found to be 0.205 nm, which is indicative of the Cu(111) lattice plane [58].

In contrast, the 5.0 wt% Cu/Al_2O_3 (S) displays large distinct particles approximately (12.8 nm) with a broad deviation of ±9.3 nm (Table 1). The larger particle size compared to the other Cu precursors used is attributed to the incomplete $CuSO_4$ decomposition to CuO after calcination, (reflections at 20.7° and 24.6° are seen in the calcined sample, Fig. 3a) resulting in the remnant $CuSO_4$ species to reduce directly to large Cu particles. The particle size distributions measured by STEM and calculated by PXRD using WPPM (Fig. 3b) were found to be consistent, considering PXRD lacked the sensitivity to detect crystallites <3 nm, due to destructive interference and a poor signal: background noise ratio. One can also observe that the simple line profile analysis via the integral breath method (used in this work) is inadequate in this system as a volume-weighted crystallite size is determined. This leads to particle sizes (assuming particles are monocrystalline) considerably larger compared to the sizes determined by STEM or WPPM.

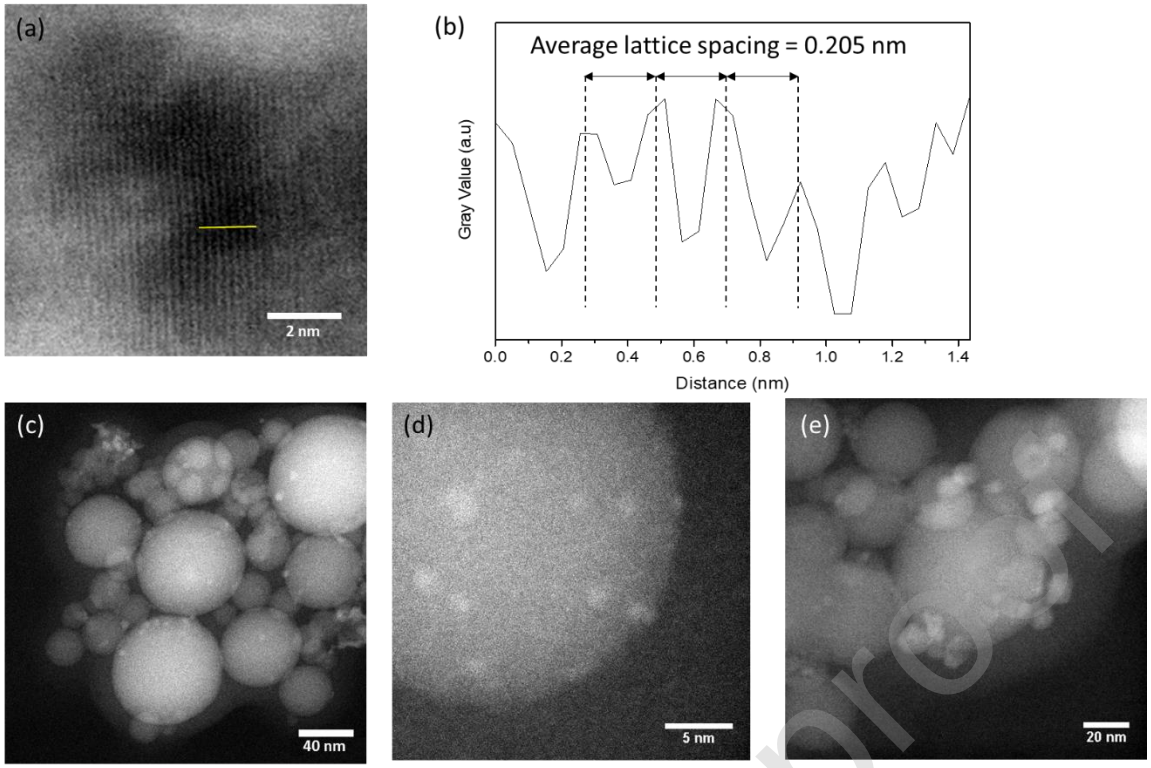

Fig. 2 Bright and Dark field STEM images and interplanar measurement of (a) 5.0 wt% Cu/Al_2O_3 (A), (b) lattice spacing of 5.0 wt% Cu/Al_2O_3, area of measurement indicated by a yellow line. (c) 5.0 wt% Cu/Al_2O_3 (A, low magnification), (d) 5.0 wt% Cu/Al_2O_3 (N) and (e) 5.0 wt% Cu/Al_2O_3 (S).

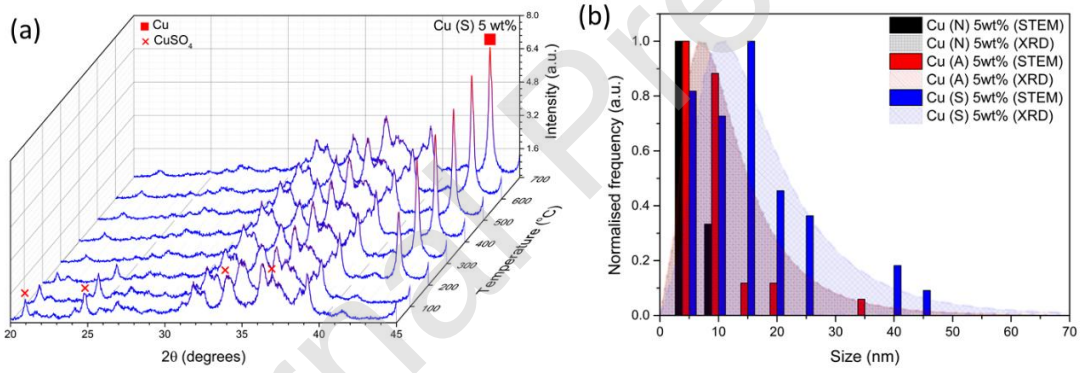

Fig. 3 (a) In-situ-PXRD patterns of 5wt% Cu/Al_2O_3 (S) catalysts reduced under 20% H_2/80% He gas flow at varying temperatures. Fig. 3 (b) Copper size distribution for 5.0 wt% Cu/Al_2O_3 catalysts after reduction. STEM (histogram) and WPPM result (lognormal distributions).

3.1.4 X-ray Photoelectron Spectroscopy (XPS) and X-ray excited Auger Electron Spectroscopy (XAES)

Fig. 4a shows XPS spectra of the ex-situ reduced catalysts along with the Cu, CuO and Cu_2O reference standards. All six catalysts show the characteristic Cu 2p doublet with the Cu $2p_{3/2}$ signal centred at 932.8 eV. The absence of strong shake-up satellites at 942.6 eV and 962.3 eV, especially for the nominal 1.0 wt% Cu/Al_2O_3 catalysts, indicate the absence of Cu^{2+} species (CuO or $CuSO_4$ compounds) and that the Cu is largely in its Cu^0 or Cu^+ oxidation state. Note

that the presence of some oxidised copper species is expected as the samples have been exposed to atmosphere prior to analysis. Catalysts with a nominal copper loading of 5.0 wt%, do show a noticeable presence of the shake-up satellite, suggesting that these materials are more oxidised than the 1.0 wt% Cu/Al_2O_3 catalysts. The Cu 2p binding energies of Cu^+ and Cu^0 are very similar, and therefore deconvolution of the spectra is often problematic. However, the chemical shift in the Auger spectra is much more prominent. Note that the L_3VV Auger spectrum of the reference Cu_2O spectrum is substantially shifted to lower kinetic energies compared to the bulk metallic Cu (Table S2). Auger spectra of the catalysts are attenuated compared to the bulk reference materials and the peaks were found to shift to lower kinetic energies.

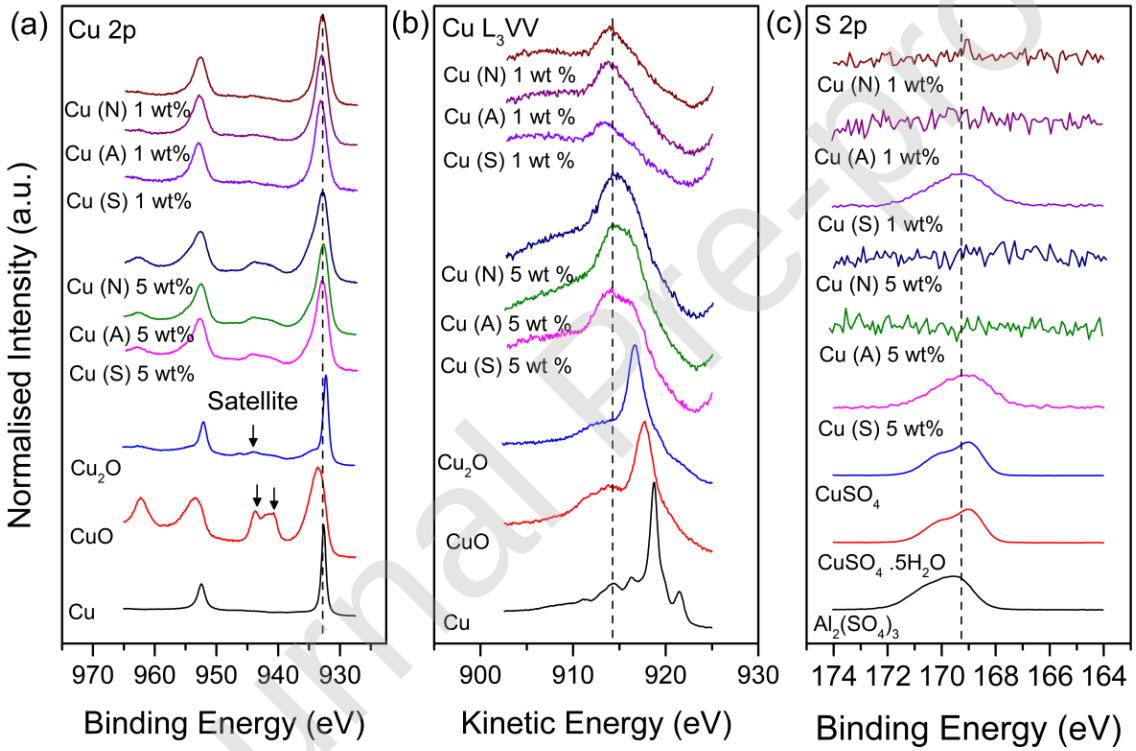

Fig. 4. High resolution stacked XPS and XAES spectra of the (a) Cu 2p, (b) Cu L_3VV and (c) S 2p regions for the six Cu/Al_2O_3 catalysts after calcination and reduction at 500 °C and 300 °C respectively. Reference spectra of the Cu, CuO and Cu_2O $Al(SO_4)_3$, $CuSO_4 .5H_2O$ and $CuSO_4$ are also presented.

The observation that the binding energies, Auger lines and consequently the modified Auger parameter, α' are sensitive to interactions between the metal and the support, as well as the particle size, has been reported previously in the literature [59-62]. The modified Auger parameter depends both on initial and final state effects and can provide an estimate of the relaxation energy/screening in the presence of core holes [63], while not suffering from

charging and calibration problems [64]. A high α' indicates higher relaxation energy or improved screening energy, which can be due to a greater number of atoms screening the core-hole after photoemission when examining copper structures of different sizes or different polarizable supports. In agreement with our studies, we find the modified Auger parameter of our catalysts to be on average around 1847.0 eV, which is drastically lower than that of bulk copper (α'_{bulk} = 1851.3 eV, displayed in Table S2). We attribute this shift largely to the polarizability of the support [62]. Comparing the modified Auger parameter between catalysts of different loadings, Table S2, the α' is observed to increase with increasing copper ensemble size. A similar trend is seen in the relaxation energies in reference to the bulk copper, ΔR. All catalysts exhibit stark changes in their relaxation energies compared to bulk copper. Interestingly, the 1.0 wt% Cu/Al_2O_3 catalysts exhibit larger changes in their approximated ΔR values compared to their higher Cu loading counterparts, which is attributes to the decreasing number of Cu atoms in their nanostructures and the greater interaction with the support due to the higher dispersion (Table S1). The spectra in Fig. 4 suggest the presence of an oxidised outer surface layer comprising mostly of CuO, especially for the 5.0 wt% Cu/Al_2O_3 catalysts, and an underlying Cu^0 bulk which was confirmed by PXRD in Fig. 1. The data also supports Rhodin's findings that at room temperature oxidation occurs rapidly for the first few seconds to minutes, where a thin oxide film forms (~0.5 nm) after which the rate of oxidation drops to a negligible value [65]. In the present work, this also explains why an oxide layer is not detected in the diffractogram.

The S 2p region was also explored (Fig. 4c). The catalysts derived from copper sulphate displayed a peak at 169.2 eV, indicative of sulphate species (bulk sulphur has a binding energy of 164.0 eV) [66]. It should be noted that the in-situ PXRD experiments (Fig. 3) do not show any reflections that could be assigned to $CuSO_4$ when the catalyst is reduced at 300 °C and above, indicating that the bulk crystalline copper sulphate precursor was reduced at 300 °C. It is also known that $Al_2(SO4)_3$ could also be formed from the decomposition of $CuSO_4$ through the reaction between SO_3 and Al_2O_3 [67]. The XPS results, however, suggest that sulphate species may remain in an amorphous fashion on the copper surface at 300 °C. In contrast, the N 1s region (Fig. S3) did not show the presence of nitrate compounds in the catalysts tested in the present work, indicating the nitrate precursor decomposed fully without leaving trace nitrogen species.

3.1.5 X-ray Absorption Spectroscopy (XAS)

Linear Combination Fitting (LCF) was completed on the Cu K-edge XANES spectra (Fig. S4) with the results being summarized in Table S3. The differences in metallic Cu composition of the 5.0 wt% Cu/Al_2O_3 is attributed to differences in particle size. The larger the particle size, the lower the surface area to volume ratio and therefore less surface oxide forms. We deduce a similar conclusion for the 1.0 wt% Cu/Al_2O_3. The LCF did not reveal any metallic Cu phase, while an unsatisfactory fit was made with bulk CuO but the observed shift to higher energies in the XANES even so suggests the presence of Cu^{2+} ions, but possibly coordinated to the alumina support. EXAFS model fitting shown in Table 2 supports the previous characterisation results. The EXAFS spectra in R-space displayed in Fig. 5b shows that the 1.0 wt% Cu/Al_2O_3 catalysts lack in long-range order as the signal quickly attenuates after the Cu-O shell (1.95 Å). The coordination number of these oxidised catalysts suggests that the Cu phase is almost completely coordinated to oxygen, which is expected as the samples have been exposed to atmosphere prior to analysis. In addition, the absence of a Cu-Cu scattering path (arising from Cu-O-Cu bonds at 2.90 Å) typical for CuO, together with the XANES data suggests that the Cu atoms are likely coordinated with the oxygens on the alumina support. XAS experiments by Cheah et al. [68, 69] suggest that during the impregnation process the $Cu/\gamma\text{-}Al_2O_3$ system comprises octahedral Cu^{2+} $(O, OH)_6$ species present on the surface as monomeric, dimeric and oligomeric hydroxo-bridged with Cu-O equatorial bond lengths of 1.95 Å. Further operando XAS work by Cassinelli et al. [70] shows that once the catalyst is calcined the octahedral Cu^{2+} $(O, OH)_6$ structure remains. After reduction (250°C in an H_2/He atmosphere) however, these authors observe the reduction of Cu^{2+} species to Cu^0 and Cu^+. We propose that during the reduction of the catalyst such hydroxo-bridges break down leaving behind a metallic Cu-Cu bond, creating a paracrystalline structure (as discussed earlier) and when exposed to the atmosphere during sample transfer an oxide layer forms. The absence of Cu-Cu coordination for the 1.0 wt% catalyst (N) (Table 2) suggests the Cu atoms after reduction are atomically dispersed (single-atom catalyst) while the remaining 1.0 wt% catalysts comprise isolated/dimer Cu atoms (due to the average coordination being <1 for Cu-Cu) on the alumina's surface [41]. The 5.0 wt% Cu/Al_2O_3 (A) catalyst's Cu-Cu bond appears to be considerably more strained and lower coordination compared to its similar loaded counterparts. This suggests that the catalyst has an intermediate morphology between the other 5.0 wt% catalysts and the 1.0 wt% catalysts. The presence of sintered particles which have formed an oxide layer composed of Cu_2O (1.88 Å) and CuO (1.96 Å) can explain the smaller Cu-O bond lengths for the 5 wt%

catalysts.

Table 2 EXAFS model fitting of reduced ex-situ Cu/Al_2O_3 catalysts, Cu and CuO reference foil/powder.

Sample	Shell	CN[a]	R[b] (Å)	σ^2 (Å^2)	R factor
Cu foil	Cu-Cu	12	2.551 ± 0.054	0.0093 ± 0.0008	0.0270
CuO	Cu-O	4	1.956 ± 0.004	0.0032 ± 0.0005	0.0013
Cu/Al_2O_3 (N) 1.0 wt%*	Cu-O	3.0 ± 0.3	1.953 ± 0.010	0.0049 ± 0.0013	0.0087
Cu/Al_2O_3 (N) 1.0 wt%#	Cu-Cu	0.4 ± 0.3	2.569 ± 0.024	0.0080 ± 0.0065	
	Cu-O	3.0 ± 0.2	1.950 ± 0.007	0.0048 ± 0.0009	0.0097
Cu/Al_2O_3 (A) 1.0 wt%*#	Cu-O	2.9 ± 0.6	1.959 ± 0.020	0.0051 ± 0.0025	0.0265
Cu/Al_2O_3 (A) 1.0 wt%	Cu-Cu	0.9 ± 0.3	2.577 ± 0.011	0.0089 ± 0.0030	
	Cu-O	2.8 ± 0.2	1.950 ± 0.007	0.0049± 0.0008	0.0081
Cu/Al_2O_3 (S) 1.0 wt%*#	Cu-O	3.2 ± 0.6	1.967 ± 0.019	0.0067 ± 0.0026	0.0242
Cu/Al_2O_3 (S) 1.0 wt%	Cu-Cu	0.7 ± 0.6	2.605 ± 0.024	0.0117 ± 0.0075	
	Cu-O	3.1 ± 0.3	1.960 ± 0.010	0.0063 ± 0.0013	0.0141
Cu/Al_2O_3 (N) 5.0 wt%	Cu-Cu	3.7 ± 0.6	2.554 ± 0.012	0.0089 ± 0.0013	
	Cu-O	2.7 ± 0.6	1.919 ± 0.017	0.0092 ± 0.0032	0.0111
Cu/Al_2O_3 (A) 5.0 wt%	Cu-Cu	2.0 ± 0.4	2.564 ± 0.011	0.0085 ±0.0017	
	Cu-O	2.8 ± 0.3	1.938 ± 0.013	0.0071 ± 0.0017	0.0120
Cu/Al_2O_3 (S) 5.0 wt%	Cu-Cu	4.8 ± 0.8	2.543 ± 0.012	0.0085 ±0.0014	
	Cu-O	1.7 ± 0.7	1.884 ± 0.024	0.0118 ± 0.0083	0.0145

[a] CN, average coordination number; [b] R, the distance between the absorber and backscattered atoms. σ^2; Debye-Waller factor; R-factor, the closeness of fit. *Model assuming Cu atoms are atomically dispersed, and #model assumed not to represent Cu local environment.

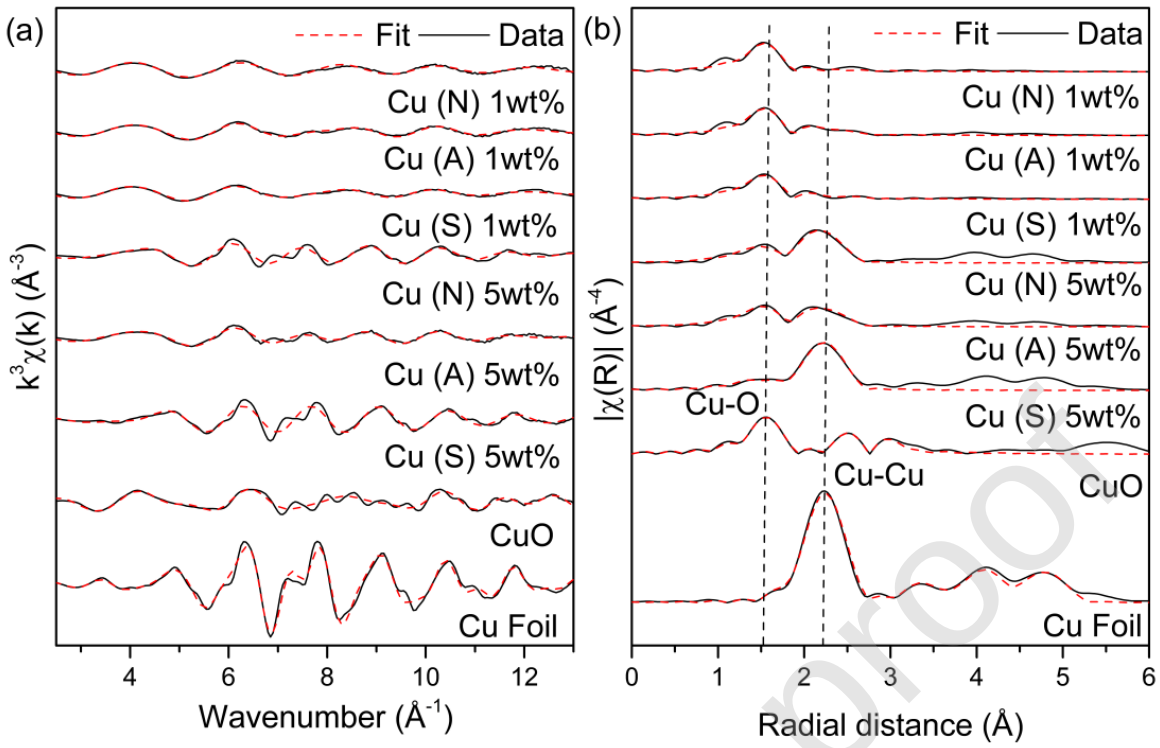

Fig. 5 (a) EXAFS spectra in k-space (k-weight = 3) and (b) R-space (k-weight = 3) for the ex-situ reduced Cu/Al_2O_3 catalysts along with Cu and CuO reference foil/powder. A k range of 3.0 – 12.8 Å was used to Fourier transform and analyse the data.

3.2 Catalytic testing

The performance of the Cu/Al_2O_3 catalysts was investigated for the hydrogenation of furfural in the liquid phase at 50 °C in MeOH at 1.5 and 10 bar of hydrogen. The conversion of furfural can follow multiple pathways, which are displayed in Scheme 1. The results of the catalytic tests are summarised in Table 3. In the absence of any solid catalyst, neither decarbonylation nor hydrogenation reactions were observed. The parent Al_2O_3 support was also found to be inactive towards the hydrogenation of furfural, favouring either the decarbonylation of furfural or the acetalization with methanol, with minimal conversion. In the case of all Cu based catalysts, the desired selective hydrogenation of furfural to furfuryl alcohol was observed alongside furan formation (Table S4). However, the target reaction of this work was the selective hydrogenation of furfural to furfuryl alcohol. Therefore, the reaction conditions were tuned to maximise the performance of the catalyst towards the hydrogenation reaction and not the decarbonylation of furfural to furan. Additionally, the catalysts derived from $CuSO_4$ were found to promote acetalization pathway, generating 2-furaldehyde dimethyl

acetal (FDMA, GCMS spectrum in Fig. S5), a high-cost molecule that can be used in subsequent reactions such as the Mukaiyama aldol reaction [71].

The conversion of furfural was observed to decrease using the materials synthesised from the following metal precursors copper acetate > copper nitrate > copper sulphate. Increasing the pressure of hydrogen was found to increase the conversion and selectivity towards furfuryl alcohol as the abundance of adsorbed hydrogen made the hydrogenation pathway more favourable over acetalization and decarbonylation. The low activity of the material synthesised from the sulphate precursor was also accompanied by the formation of furan arising from the decarbonylation of furfural and the formation of FDMA (Table 3).

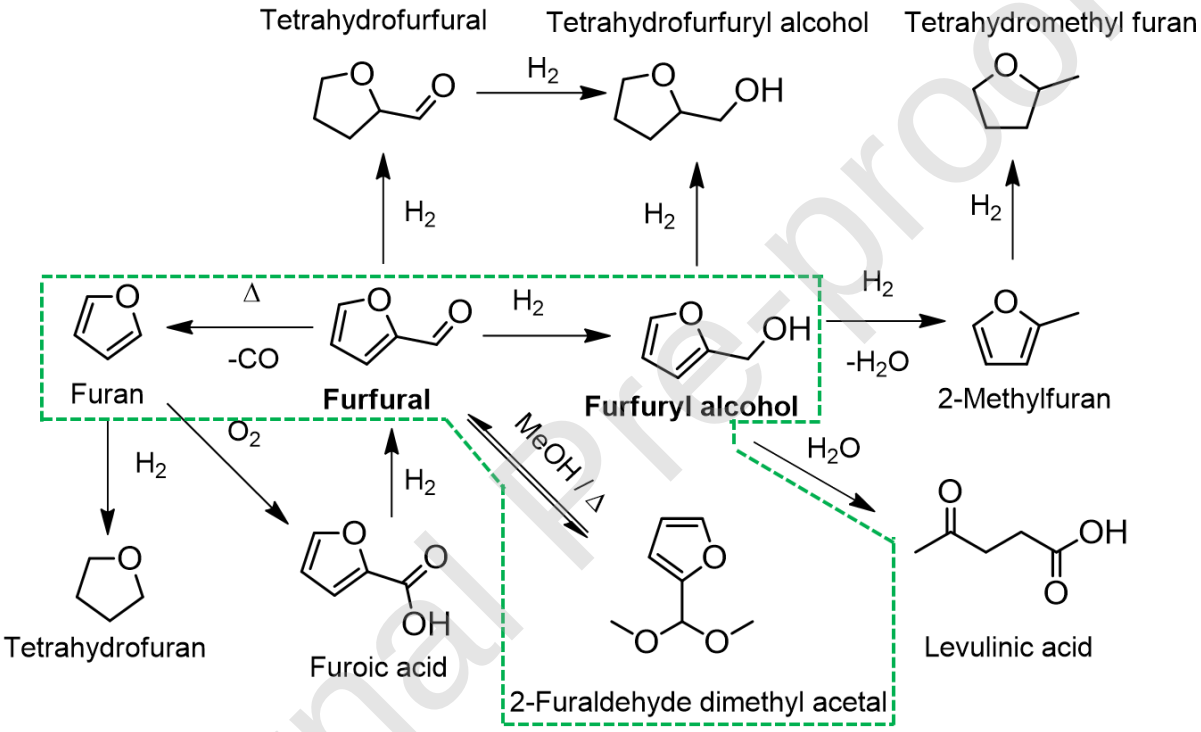

Scheme 1 Reaction scheme for upgrading furfural.[4]. Reaction pathways seen in this work is marked by the green dotted line.

Table 3 Summary of catalytic data for the hydrogenation of furfural using copper catalysts. Reaction conditions: 7 h, 50 °C, 1.5 bar and 10 bar of H_2, 600 RPM, and 30 mg of catalyst.

Cu precursor	Nominal Cu wt%	H_2 pressure (bar)	Conversion (%)	Furfuryl alcohol S (%)	Furan S (%)	FDMA S (%)
Nitrate	1.0	1.5	9.2 ± 0.5	86.3 ± 4.3	13.7 ± 0.7	0
	5.0		14.1 ± 0.7	94.6 ± 4.7	5.4 ± 0.3	0
	1.0	10	99.3 ± 5.0	99.8 ± 5.0	0.2 ± 0.1	0
	5.0		99.0 ± 5.0	99.5 ± 5.0	0.5 ± 0.1	0
Acetate	1.0	1.5	24.2 ± 1.2	96.0 ± 4.8	4.0 ± 0.2	0
	5.0		47.7 ± 2.4	97.6 ± 4.9	2.4 ± 0.1	0
	1.0	10	99.0 ± 5.0	99.8 ± 5.0	0.2 ± 0.1	0
	5.0		99.4 ± 5.0	99.6 ± 5.0	0.4 ± 0.1	0
Sulphate	1.0	1.5	2.2 ± 0.1	5.1 ± 0.3	61.4 ± 3.1	33.5 ± 1.7
	5.0		7.8 ± 0.4	0.8 ± 0.1	11.3 ± 0.6	89 ± 4.5
	1.0	10	94.9 ± 4.7	94.7 ± 4.7	0.3 ± 0.1	5.1 ± 0.3
	5.0		91.8 ± 4.6	83.5 ± 4.2	0.9 ± 0.1	15.6 ± 0.8

The reaction profiles of the 1.0 wt% Cu/Al_2O_3 catalysts at a mild pressure of 1.5 bar (Fig. 6a) indicates the presence of an induction period of 5 to 6 h where the catalysts are mostly inactive in terms of conversion and furfural alcohol production; more evident for Cu/Al_2O_3 (N) and Cu/Al_2O_3 (A) catalysts. Furthermore, when performing the reaction at a higher hydrogen pressure of 10 bar, the induction period is reduced to ~1 h (Fig. 6b). This behaviour is believed to be due to the formation of surface oxide on the copper surface from oxygen contamination. A more rigorous reduction procedure was followed (320 °C for 0.5 h) which had no effect on the induction period, so we assume pre-dissolved oxygen in the reaction mixture temporarily disabled the catalyst. DFT calculations [72] show that CuO is unable to produce atomic hydrogen which would enable hydrogenation reactions until the oxide had been reduced. As expected the induction period also depends on the partial pressure of hydrogen used in the reaction, as in hydrogen-rich conditions CuO completely reduces into metallic Cu without the formation of suboxides (i.e., Cu_2O or Cu_4O_3) which hinder the rate of reduction [73].

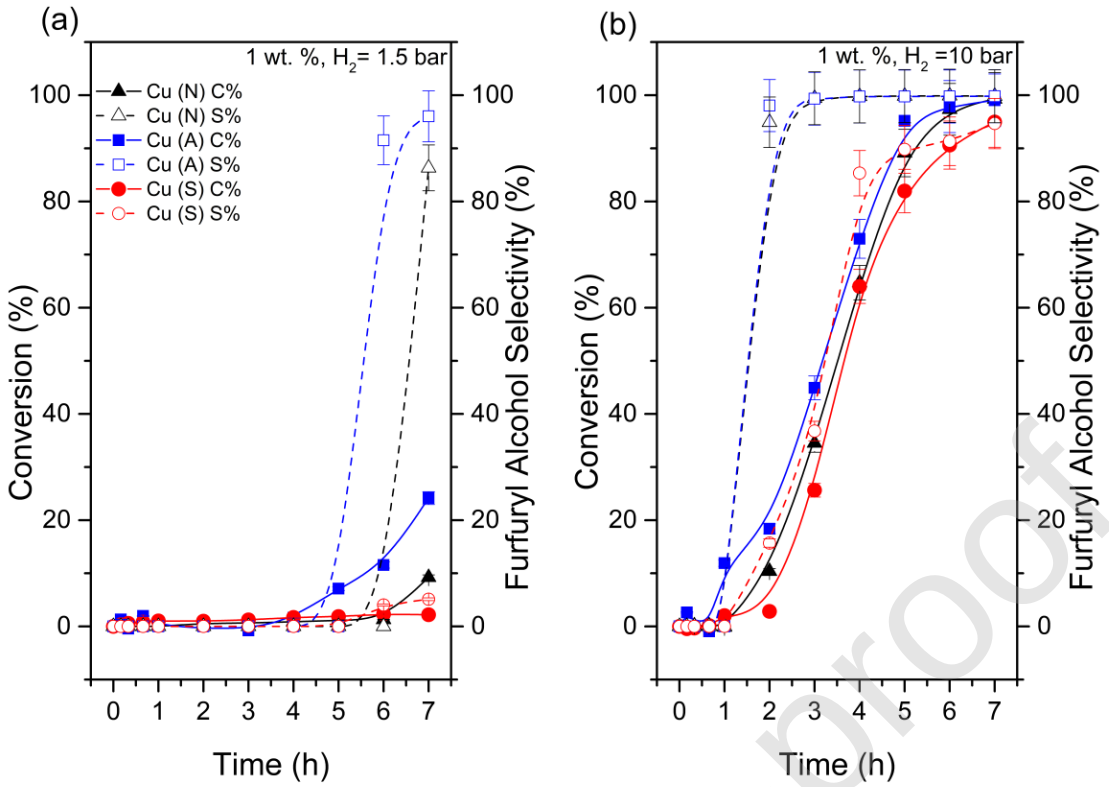

Fig. 6 The reaction profiles of furfural conversion and furfuryl alcohol selectivity. Reaction conditions: 50 °C, (a) 1.5 bar and (b) 10 bar of H_2, 600 RPM, 30 mg of catalyst and using supported 1 wt% Cu/Al_2O_3 catalysts. Solid and dashed lines represent the conversion and selectivity to furfuryl alcohol, respectively.

Fig. 7 presents the reaction profiles of the 5.0 wt% Cu/Al_2O_3 catalysts. Clearly, the Cu/Al_2O_3 (S), shows poorer selectivity towards furfuryl alcohol with the difference being more evident when operating the reaction at 1.5 bar of H_2. This behaviour is thought to be due to deactivation of the surface from the remnant sulphur species (mainly sulphate), which is present from the XPS analysis (Fig. 4c). The deactivation mentioned is most likely related to the presence of S which is more electronegative than Cu, thus withdrawing electron density from the surface and causing a modification to the electronic surface [74]. It is worth mentioning that a simulation study conducted by Kitchin et al. [75], determined that sulphur preferentially adsorbs onto the high surface energy and high co-ordinated FCC and HCP sites on the copper surface, hydrogen also preferentially adsorbs to these sites [76, 77]. The presence of sulphur passivates copper's ability to chemisorb hydrogen, where the process already activated (requires energy) [78] unlike other metals such as Pd, Pt and Ni [79]. Surface electron density alteration allows side reactions such as the formation of furan and FDMA to be preferred (displayed by the immediate increase in conversion in Fig. 7b). Consequently, the selectivity is seen to flip towards furfuryl

alcohol when the partial pressure of hydrogen is increased (Fig. 6b and Fig. 7b) as the rate-determining step is no longer hydrogen adsorption.

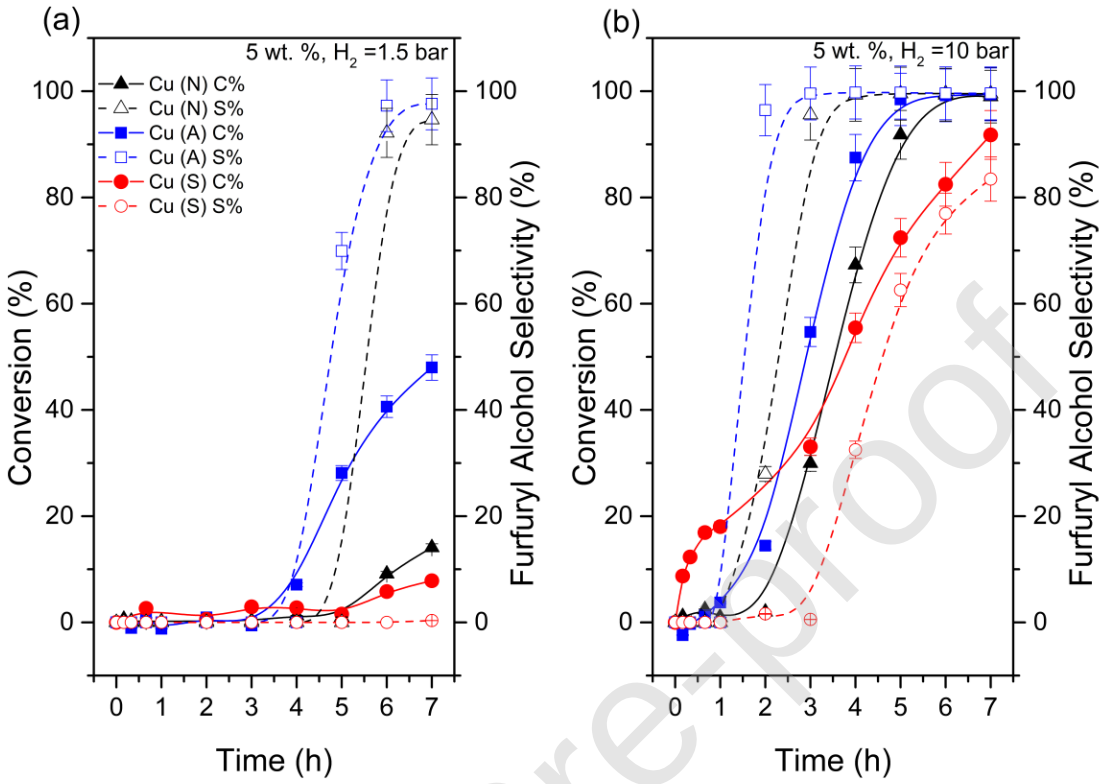

Fig. 7. The reaction profiles of furfural conversion and furfuryl alcohol selectivity. Reaction conditions: 7 h, 50 °C, (a) 1.5 bar and (b) 10 bar of H_2, 600 RPM, 30 mg of catalyst and using supported 5 wt% Cu/Al_2O_3 catalysts. Solid and dashed lines represent the conversion and selectivity to furfuryl alcohol, respectively.

Commonly reported in the literature [3, 80-85], the acetalization of aldehydes, including furfural (Scheme S1), in alcoholic solvents is observed. The acetalization process is achieved with alcohols in the presences of Lewis [84, 85] or protic [84] acid catalysts. The acetalization of furfural with alcohol solvents was also reported using supported Pt catalysts by Taylor et al. [3]. The authors found that the hydrogenation of furfural is sensitive to the selection of the solvent with ethanol favouring the formation of the undesired acetal product, though using solvents such as methanol at lower temperatures was found to suppress the side reaction.

The significant formation of FDMA with the sulphate-derived catalysts (Table 4) was attributed to the presence of sulphate species which catalyses the acetalization of furfural and methanol which to best of our knowledge has not been demonstrated for this reaction. To investigate this further we have utilised the two possible forms of metal sulphates that may be present in the sulphur-derived catalyst. The bulk $Al_2(SO_4)_3$ catalyst is shown to be the most active catalyst with it immediately catalysing the reaction at room temperature with minimal

agitation (conversion = 92.7%). We attribute this extraordinary activity and selectivity due to the 'super Lewis acid sites' [86] and possibly homogeneous catalytic character as this was the only catalyst found to be dissolved in methanol at the end of the experiment. Similarly, the bulk $CuSO_4$ and the non-reduced 5.0 wt% Cu/Al_2O_3 (S) ($CuSO_4$ reflections observed in Fig. 3) was found extremely-active and selective for the acetalization reactions at 50 °C (Table 4). Note that at a reduction temperature of 200 °C, the sulphur-derived catalyst has both the features of $CuSO_4$ and metallic Cu (Fig. 3) while the sulphur-free 5.0 wt% Cu/Al_2O_3 (A) catalyst only has metallic Cu reflections (Fig. S6). Our results indicate that the presence of sulphate species in the catalyst can direct the reaction towards acetalization. Furthermore, leaching of the sulphur was confirmed through ICP-OES analysis of the supernatant fluid after ageing the sulphate-derived catalyst in MeOH at 50 °C for 7 h. Under the same experimental conditions, the supernatant fluid and the resulting "cleaned" catalyst were still able to promote the acetalization reaction through via a homogeneous route (Table 4 and Fig. S7).

Table 4 Summary of catalytic data for the acetalization of furfural using sulphate and sulphate-free catalysts. Reaction conditions: 7 h, 50 °C, 1.5 bar, 600 RPM, and 30 mg of catalyst.

Catalyst	Reduction temperature (°C)	Conversion (%)	Furfuryl alcohol S (%)	Furan S (%)	FDMA S (%)
$Al_2(SO_4)_3$	n/a	84.5 ± 4.2	0	0	100 ± 5.0
$CuSO_4$	n/a	89.6 ± 4.5	0	0	100 ± 5.0
Cu/Al_2O_3 (S) 5.0 wt%	n/a	94.0 ± 4.7	0	0	100 ± 5.0
Cu/Al_2O_3 (S) 5.0 wt%	200	95.8 ± 4.8	2.3 ± 0.1	0	97.7 ± 4.9
Cu/Al_2O_3 (A) 5.0 wt%	200	34.0 ± 1.7	98.6 ± 4.9	0	1.4 ± 0.1
Cu/Al_2O_3 (S) 5.0 wt%	300	7.8 ± 0.4	0.8 ± 0.1	11.3 ± 0.6	89.0 ± 4.5
Cu/Al_2O_3 (S) 5.0 wt% cleaned*	n/a	70.5 ± 3.5	36.4 ± 1.8	0	63.6 ± 3.2
Supernatant fluid	n/a	93.1 ± 4.7	0	0	100 ± 5.0

*Catalyst was washed in methanol at 50 °C for 7h before use.

Increasing the copper loading of the catalyst and consequently increasing the size of the Cu ensembles leads to improved conversions and selectivity towards furfuryl alcohol for all the sulphur-free catalysts at low hydrogen pressures (Table 3). The increased conversion can be explained by the higher copper content and availability of active sites for hydrogen adsorption. At higher pressures, this limiting factor is removed for the 1.0 wt% catalysts. Fig. 8 shows that the 1.0 wt% catalysts are superior in all cases in terms of catalytic activity when normalised to metal content. Turnover frequencies were calculated using dispersions calculated from XPS (Table S1). TOFs in Table S5 show that the surface Cu sites in 1.0 wt% catalysts typically better, possibly due to their lack of coordination and higher reactivity for the conversion of

furfural. TOFs also support our finding that at low hydrogen partial pressures, sulphur containing catalyst has inferior active sites compared to their sulphur-free counterparts.

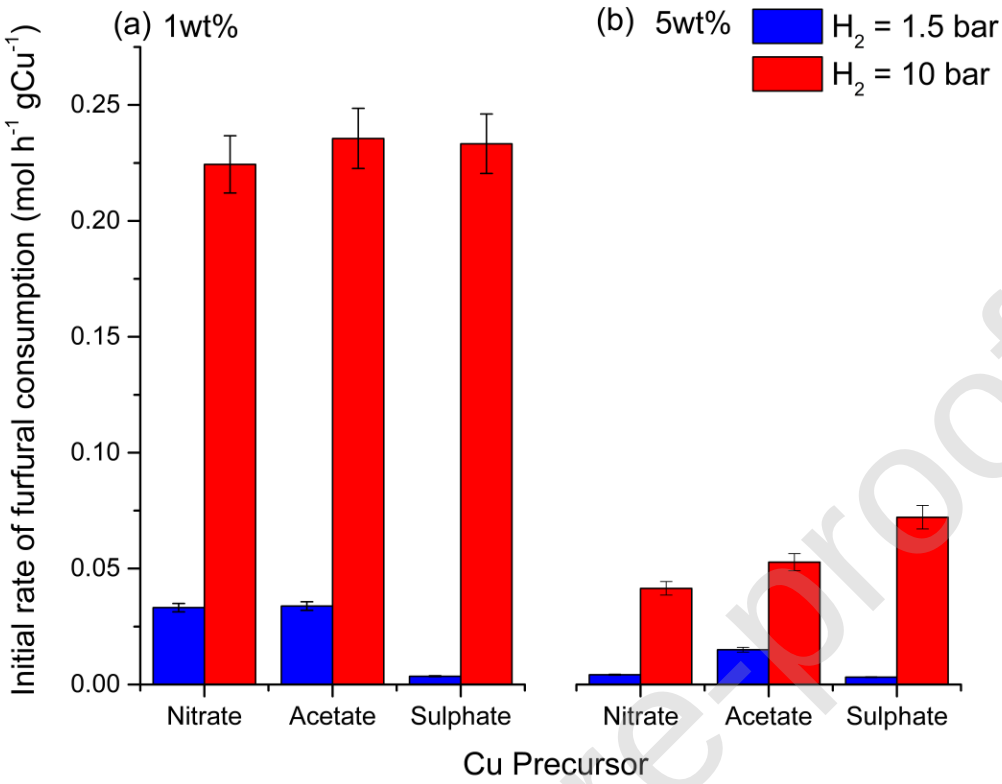

Fig. 8. Normalised initial rates of furfural consumption per gram of Cu after the induction period across (a) 1.0 wt% and (b) 5.0 wt% Cu/Al_2O_3 catalysts at differing hydrogen pressures.

Table 3 shows that across all the catalyst series and at low hydrogen pressures, the selectivity towards furan is inversely proportional to the Cu loading which suggests that the reaction is structure sensitive and depends on the Cu morphology. This has been previously reported by Pushkarev et al. [87] using supported monometallic platinum catalysts. The authors found that smaller Pt nanoparticles (1.5 nm) were more adept to access the decarbonylation pathway, while larger particles (7.1 nm) increased the selectivity towards furfuryl alcohol. We suggest that a similar behaviour is in place in the present case. It has been shown that Cu (111) surfaces interact with furfural via the lone pair on the oxygen atom of the carbonyl group to produce the perpendicular η^1(O)-aldehyde conformation [4, 21, 25, 26]. Sitthisa et al. [26] suggest this is due to the repulsion of the furan ring from the closely packed Cu (111) surface due to an overlap of the 3d band of the Cu surface atoms with the anti-bonding orbital of the aromatic furan ring. The adsorption of furfural via this η^1(O)-aldehyde mode and the instability of the η^2(C, O)-aldehyde conformation is thought to be the reason why Cu surfaces typically favour the hydrogenation of the C=O bond over the decarbonylation reactions observed in Pd catalysts

[24]. Typically, as the size of the metal ensembles decreases, the presence of lower coordination facets is favoured (such as the Cu (100) and Cu (110) surfaces). DFT calculations by Sitthisa et al. [26], suggests that more open Cu (110) surfaces allows the furan ring to move closer to the surface because of the lower density of Cu atoms that can interact with the aromatic ring. Consequently, the 5.0 wt% catalysts (N and A) are very selective towards furfuryl alcohol at low pressures. As the ensemble size decreases with the 1.0 wt% catalysts (N and A) the selectivity towards decarbonylation reactions increase as repulsion of the furan ring falls due to the formation of isolated and dimer Cu species.

The recyclability of the 1 wt% and 5 wt% catalyst derived from the acetate precursor was also investigated. The catalyst was recovered after the reaction via centrifugation followed by washing with methanol. Once dried, it was found that 15% of the catalyst was lost during the recovery. This was subsequently retested under optimal conditions by downscaling the reaction volume by the same ratio. Table 5 shows that the activity and selectivity remain unchanged after the recycling test for both catalysts.

Table 5 Furfural hydrogenation over recycled catalysts. Reaction conditions: 4 h, 50 °C, 10 bar of H_2 and 600 RPM.

Catalyst	Nominal Cu (wt%)	Hydrogen Pressure (bar)	Conversion (%)	Furfuryl Alcohol S (%)	Furan S (%)	FDMA S (%)
^{1}Cu/ Al_2O_3 (A)	1.0	10	73.0 ± 3.7	99.8 ± 5.0	0.2 ± 0.1	0
^{2}Cu/ Al_2O_3 (A)	1.0	10	72.4 ± 3.6	99.2 ± 5.0	0.8 ± 0.1	0
^{1}Cu/ Al_2O_3 (A)	5.0	10	87.5 ± 4.4	99.8 ± 5.0	0.2 ± 0.1	0
^{2}Cu/ Al_2O_3 (A)	5.0	10	86.3 ± 4.3	99.6 ± 5.0	0.4 ± 0.1	0

Superscripts 1 and 2 indicate the catalyst cycle of testing.

4 Conclusions

The copper catalysed liquid phase hydrogenation of furfural was studied over a series of supported monometallic Cu/Al_2O_3 catalysts synthesised via different Cu precursors using a simple wet impregnation method which is relatively easy to scale up. The catalyst morphology and electronic properties were examined via STEM, EXAFS, PXRD, XPS, XAES, ICP-OES and BET. Furfural hydrogenation was found susceptible to the presence of sulphates in the catalyst, entirely altering the selectivity to the acetalization pathway of furfural with methanol at over 90% conversion under mild conditions. Catalytic tests show that the sulphate impurities deactivate the catalyst leading to lower conversion and altered selectivities at near ambient hydrogen pressures. We have also demonstrated that the selective furfural hydrogenation can be structure sensitive as isolated and dimer Cu atoms were found to promote decarbonylation reactions due to their lower packed copper structure which influences the interaction of the

furan ring with the underlying surface; mimicking platinum group catalysts. In all cases catalysts derived from copper acetate were found to be superior in all cases, suggesting the metal precursor selection appears to be critical to achieving optimal catalytic activity. The mechanism of the precursor decomposition and anchoring onto the support plays a substantial role in the final catalytically active copper morphology and the development of a cheap, non-toxic and selective catalyst.

Author contributions

M. J. Islam, A. Osatiashtiani, J. C. Manayil, C. M. A. Parlett, M. A. Isaacs, and G. Kyriakou contributed to the experimental work. M. J. Islam, M. Granollers Mesa, A. Osatiashtiani, M. J. Taylor, G. Kyriakou performed the data analysis. The paper was written by M. J. Islam, M. Granollers Mesa, M. J. Taylor and G. Kyriakou.

Declaration of interests

The authors declare that they have no known competing financial interests or personal relationships that could have appeared to influence the work reported in this paper.

Acknowledgements

The authors wish to acknowledge the Diamond Light Source and the UK Catalysis Hub for provision of beamtime (proposal number SP19850-1). MJI acknowledges the award of a PhD scholarship from Aston University. The authors also acknowledge the Energy Research Accelerator (ERA) for the funding of equipment used in this work. GK acknowledges funding from EPSRC (EP/M005186/2) and funding by the University of Patras Research Committee under the basic research program K. Karatheodoris.

References

[1] D.M. Alonso, J.Q. Bond, J.A. Dumesic, Catalytic conversion of biomass to biofuels, Green Chem., 12 (2010) 1493-1513.
[2] J.H. Clark, V. Budarin, F.E.I. Deswarte, J.J.E. Hardy, F.M. Kerton, A.J. Hunt, R. Luque, D.J. Macquarrie, K. Milkowski, A. Rodriguez, O. Samuel, S.J. Tavener, R.J. White, A.J. Wilson, Green chemistry and the biorefinery: A partnership for a sustainable future, Green Chem., 8 (2006) 853-860.
[3] M.J. Taylor, L.J. Durndell, M.A. Isaacs, C.M.A. Parlett, K. Wilson, A.F. Lee, G. Kyriakou, Highly selective hydrogenation of furfural over supported Pt nanoparticles under mild conditions, Appl. Catal., B, 180 (2016) 580-585.
[4] X. Li, P. Jia, T. Wang, Furfural: A Promising Platform Compound for Sustainable Production of C4 and C5 Chemicals, ACS Catal., 6 (2016) 7621-7640.
[5] B.M. Matsagar, S.A. Hossain, T. Islam, H.R. Alamri, Z.A. Alothman, Y. Yamauchi, P.L. Dhepe, K.C.W. Wu, Direct Production of Furfural in One-pot Fashion from Raw Biomass Using Brønsted Acidic Ionic Liquids, Sci. Rep., 7 (2017) 13508.
[6] H.J. Brownlee, C.S. Miner, Industrial Development of Furfural, Ind. Eng. Chem., 40 (1948) 201-204.
[7] A. Mandalika, L. Qin, T.K. Sato, T. Runge, Integrated biorefinery model based on production of furans using open-ended high yield processes, Green Chem., 16 (2014) 2480-2489.
[8] K. Yan, G. Wu, T. Lafleur, C. Jarvis, Production, properties and catalytic hydrogenation of furfural to fuel additives and value-added chemicals, Renew. Sust. Energ. Rev., 38 (2014) 663-676.
[9] F. Ullmann, Ullmann's encyclopedia of industrial chemistry, 7th ed. ed., Wiley-VCH ;, Weinheim, Germany :, 2009.
[10] J.A. Brydson, 28 - Furan Resins, in: J.A. Brydson (Ed.) Plastics Materials (Seventh Edition), Butterworth-Heinemann, Oxford, 1999, pp. 810-813.
[11] D. Liu, D. Zemlyanov, T. Wu, R.J. Lobo-Lapidus, J.A. Dumesic, J.T. Miller, C.L. Marshall, Deactivation mechanistic studies of copper chromite catalyst for selective hydrogenation of 2-furfuraldehyde, J. Catal., 299 (2013) 336-345.
[12] R. Rao, A. Dandekar, R.T.K. Baker, M.A. Vannice, Properties of Copper Chromite Catalysts in Hydrogenation Reactions, J. Catal., 171 (1997) 406-419.

[13] H. Adkins, R. Connor, The catalytic hydrogenation of organic compounds over copper chromite, JACS, 53 (1931) 1091-1095.
[14] R. Prasad, P. Singh, Applications and Preparation Methods of Copper Chromite Catalysts: A Review, Bulletin of Chemical Reaction Engineering and Catalysis, 6 (2011) 63-114.
[15] J.J. Musci, A.B. Merlo, M.L. Casella, Aqueous phase hydrogenation of furfural using carbon-supported Ru and RuSn catalysts, Catal. Today, 296 (2017) 43-50.
[16] S. Liu, Y. Amada, M. Tamura, Y. Nakagawa, K. Tomishige, One-pot selective conversion of furfural into 1,5-pentanediol over a Pd-added Ir-ReOx/SiO_2 bifunctional catalyst, Green Chem., 16 (2014) 617-626.
[17] M. Lesiak, M. Binczarski, S. Karski, W. Maniukiewicz, J. Rogowski, E. Szubiakiewicz, J. Berlowska, P. Dziugan, I. Witońska, Hydrogenation of furfural over Pd–Cu/Al_2O_3 catalysts. The role of interaction between palladium and copper on determining catalytic properties, J. Mol. Catal. A: Chem., 395 (2014) 337-348.
[18] M.G. Dohade, P.L. Dhepe, Efficient hydrogenation of concentrated aqueous furfural solutions into furfuryl alcohol under ambient conditions in presence of PtCo bimetallic catalyst, Green Chem., 19 (2017) 1144-1154.
[19] H. Li, H. Luo, L. Zhuang, W. Dai, M. Qiao, Liquid phase hydrogenation of furfural to furfuryl alcohol over the Fe-promoted Ni-B amorphous alloy catalysts, J. Mol. Catal. A: Chem., 203 (2003) 267-275.
[20] Y. Wang, Y. Miao, S. Li, L. Gao, G. Xiao, Metal-organic frameworks derived bimetallic Cu-Co catalyst for efficient and selective hydrogenation of biomass-derived furfural to furfuryl alcohol, Mol. Catal., 436 (2017) 128-137.
[21] Y. Shi, Y. Zhu, Y. Yang, Y.-W. Li, H. Jiao, Exploring Furfural Catalytic Conversion on Cu(111) from Computation, ACS Catal., 5 (2015) 4020-4032.
[22] M.J. Taylor, L. Jiang, J. Reichert, A.C. Papageorgiou, S.K. Beaumont, K. Wilson, A.F. Lee, J.V. Barth, G. Kyriakou, Catalytic Hydrogenation and Hydrodeoxygenation of Furfural over Pt(111): A Model System for the Rational Design and Operation of Practical Biomass Conversion Catalysts, J. Phys. Chem. C, 121 (2017) 8490-8497.
[23] S. Sitthisa, W. An, D.E. Resasco, Selective conversion of furfural to methylfuran over silica-supported NiFe bimetallic catalysts, J. Catal., 284 (2011) 90-101.
[24] V. Vorotnikov, G. Mpourmpakis, D.G. Vlachos, DFT Study of Furfural Conversion to Furan, Furfuryl Alcohol, and 2-Methylfuran on Pd(111), ACS Catal., 2 (2012) 2496-2504.
[25] R. Mariscal, P. Maireles-Torres, M. Ojeda, I. Sadaba, M. Lopez Granados, Furfural: a renewable and versatile platform molecule for the synthesis of chemicals and fuels, Energy Environ. Sci, 9 (2016) 1144-1189.
[26] S. Sitthisa, T. Sooknoi, Y. Ma, P.B. Balbuena, D.E. Resasco, Kinetics and mechanism of hydrogenation of furfural on Cu/SiO_2 catalysts, J. Catal., 277 (2011) 1-13.
[27] S. Srivastava, P. Mohanty, J.K. Parikh, A.K. Dalai, S.S. Amritphale, A.K. Khare, Cr-free Co–Cu/SBA-15 catalysts for hydrogenation of biomass-derived α-, β-unsaturated aldehyde to alcohol, Chin. J. Catal., 36 (2015) 933-942.
[28] D. Kubička, P. Šimáček, N. Žilková, Transformation of Vegetable Oils into Hydrocarbons over Mesoporous-Alumina-Supported CoMo Catalysts, Top. Catal., 52 (2009) 161-168.
[29] D. Kubička, L. Kaluža, Deoxygenation of vegetable oils over sulfided Ni, Mo and NiMo catalysts, Appl. Catal., A, 372 (2010) 199-208.
[30] B. Hočevar, M. Grilc, M. Huš, B. Likozar, Mechanism, ab initio calculations and microkinetics of hydrogenation, hydrodeoxygenation, double bond migration and cis–trans isomerisation during hydrotreatment of C6 secondary alcohol species and ketones, Appl. Catal., B, 218 (2017) 147-162.

[31] B. Hočevar, M. Grilc, M. Huš, B. Likozar, Mechanism, ab initio calculations and microkinetics of straight-chain alcohol, ether, ester, aldehyde and carboxylic acid hydrodeoxygenation over Ni-Mo catalyst, Chem. Eng. J., 359 (2019) 1339-1351.
[32] X. Wang, R.Y. Saleh, U.S. Ozkan, Reaction network of aldehyde hydrogenation over sulfided Ni–Mo/Al_2O_3 catalysts, J. Catal., 231 (2005) 20-32.
[33] K.W. Cheah, M.J. Taylor, A. Osatiashtiani, S.K. Beaumont, D.J. Nowakowski, S. Yusup, A.V. Bridgwater, G. Kyriakou, Monometallic and bimetallic catalysts based on Pd, Cu and Ni for hydrogen transfer deoxygenation of a prototypical fatty acid to diesel range hydrocarbons, Catal. Today, (2019).
[34] G.J. Hutchings, F. King, I.P. Okoye, M.B. Padley, C.H. Rochester, Modification of Selectivity in the Hydrogenation of Crotonaldehyde Using Cu/Al_2O_3 Catalysts Modified with Sulfur Compounds: Effect of Sulfur Source, J. Catal., 148 (1994) 464-469.
[35] M.E. Chiu, G. Kyriakou, F.J. Williams, D.J. Watson, M.S. Tikhov, R.M. Lambert, Sulfur, normally a poison, strongly promotes chemoselective catalytic hydrogenation: stereochemistry and reactivity of crotonaldehyde on clean and S-modified Cu(111), ChemComm, (2006) 1283-1285.
[36] M.V. Twigg, M.S. Spencer, Deactivation of supported copper metal catalysts for hydrogenation reactions, Appl. Catal., A, 212 (2001) 161-174.
[37] G.J. Hutchings, F. King, I.P. Okoye, C.H. Rochester, Influence of sulphur poisoning of copper/alumina catalyst on the selective hydrogenation of crotonaldehyde, Appl. Catal., A, 83 (1992) L7-L13.
[38] G.J. Hutchings, F. King, I.P. Okoye, M.B. Padley, C.H. Rochester, Selectivity Enhancement in the Hydrogenation of α, β-Unsaturated Aldehydes and Ketones Using Thiophene-Modified Catalysts, J. Catal., 148 (1994) 453-463.
[39] M.E. Chiu, D.J. Watson, G. Kyriakou, M.S. Tikhov, R.M. Lambert, Tilt the Molecule and Change the Chemistry: Mechanism of S-Promoted Chemoselective Catalytic Hydrogenation of Crotonaldehyde on Cu(111), Angew. Chem. Int. Ed., 45 (2006) 7530-7534.
[40] M. May, S. Gonzalez, F. Illas, A systematic density functional study of ordered sulfur overlayers on Cu(111) and Ag(111): Influence of the adsorbate coverage, Surf. Sci., 602 (2008) 906-913.
[41] G. Centi, S. Perathoner, Nature of active species in copper-based catalysts and their chemistry of transformation of nitrogen oxides, Appl. Catal., A, 132 (1995) 179-259.
[42] S.W. Gaarenstroom, N. Winograd, Initial and final state effects in the ESCA spectra of cadmium and silver oxides, J. Chem. Phys., 67 (1977) 3500-3506.
[43] G. Moretti, Auger parameter and Wagner plot in the characterization of chemical states by X-ray photoelectron spectroscopy: a review, JESRP, 95 (1998) 95-144.
[44] P.W. Park, J.S. Ledford, The influence of surface structure on the catalytic activity of alumina supported copper oxide catalysts. Oxidation of carbon monoxide and methane, Appl. Catal., B, 15 (1998) 221-231.
[45] F.P.J.M. Kerkhof, J.A. Moulijn, Quantitative analysis of XPS intensities for supported catalysts, The Journal of Physical Chemistry, 83 (1979) 1612-1619.
[46] H. Shinotsuka, S. Tanuma, C.J. Powell, D.R. Penn, Calculations of electron inelastic mean free paths. X. Data for 41 elemental solids over the 50 eV to 200 keV range with the relativistic full Penn algorithm, Surf. Interface Anal., 47 (2015) 871-888.
[47] P. Scardi, M. Leoni, Whole powder pattern modelling, AcCrA, 58 (2002) 190-200.
[48] P. Scardi, M. Leoni, M. D'Incau, Whole Powder Pattern Modelling of cubic metal powders deformed by high energy milling, Z. Kristallogr. Cryst. Mater., 222 (2007) 129.
[49] M. Leoni, T. Confente, P. Scardi, PM2K: A flexible program implementing Whole Powder Pattern Modelling, Z. Kristallogr. Suppl., 23 (2006) 249-254.

[50] G. Caglioti, A. Paoletti, F.P. Ricci, On resolution and luminosity of a neutron diffraction spectrometer for single crystal analysis, NucIM, 9 (1960) 195-198.
[51] D.R. Black, D. Windover, M.H. Mendenhall, A. Henins, J. Filliben, J.P. Cline, Certification of Standard Reference Material 1976B, PDiff, 30 (2015) 199-204.
[52] B. Ravel, M. Newville, ATHENA, ARTEMIS, HEPHAESTUS: data analysis for X-ray absorption spectroscopy using IFEFFIT, J. Synchrotron Radiat., 12 (2005) 537-541.
[53] J. Ghose, A. Kanungo, Studies on the thermal decomposition of $Cu(NO_3)_2 \cdot 3\ H_2O$, J. Therm. Anal., 20 (1981) 459-462.
[54] Z. Lin, D. Han, S. Li, Study on thermal decomposition of copper(II) acetate monohydrate in air, JTAC, 107 (2012) 471-475.
[55] F. Habashi, S.A. Mikhail, K.V. Van, Reduction of sulfates by hydrogen, Can. J. Chem., 54 (1976) 3646-3650.
[56] Y. Yang, D. Xu, Q. Wu, P. Diao, Cu_2O/CuO Bilayered Composite as a High-Efficiency Photocathode for Photoelectrochemical Hydrogen Evolution Reaction, Sci. Rep., 6 (2016) 35158.
[57] M.C. Marion, E. Garbowski, M. Primet, Physicochemical properties of copper oxide loaded alumina in methane combustion, J. Chem. Soc., Faraday Trans., 86 (1990) 3027-3032.
[58] R.G. Haverkamp, A.T. Marshall, D. van Agterveld, Pick your carats: nanoparticles of gold–silver–copper alloy produced in vivo, JNR, 9 (2007) 697-700.
[59] J.P. Espinós, J. Morales, A. Barranco, A. Caballero, J.P. Holgado, A.R. González-Elipe, Interface Effects for Cu, CuO, and Cu_2O Deposited on SiO_2 and ZrO_2. XPS Determination of the Valence State of Copper in Cu/SiO_2 and Cu/ZrO_2 Catalysts, J. Phys. Chem. B, 106 (2002) 6921-6929.
[60] O.P.H. Vaughan, G. Kyriakou, N. Macleod, M. Tikhov, R.M. Lambert, Copper as a selective catalyst for the epoxidation of propene, J. Catal., 236 (2005) 401-404.
[61] Y.T. Wu, E. Garfunkel, T.E. Madey, Initial stages of Cu growth on ordered Al_2O_3 ultrathin films, J. Vac. Sci. Technol., A, 14 (1996) 1662-1667.
[62] J. Batista, A. Pintar, J.P. Gomilšek, A. Kodre, F. Bornette, On the structural characteristics of γ-alumina-supported Pd–Cu bimetallic catalysts, Appl. Catal., A, 217 (2001) 55-68.
[63] A. Thøgersen, S. Diplas, J. Mayandi, T. Finstad, A. Olsen, J.F. Watts, M. Mitome, Y. Bando, An experimental study of charge distribution in crystalline and amorphous Si nanoclusters in thin silica films, JAP, 103 (2008) 024308.
[64] S. Hofmann, Auger- and X-Ray Photoelectron Spectroscopy in Materials Science: A User-Oriented Guide, Springer Berlin Heidelberg2012.
[65] T.N. Rhodin, Low Temperature Oxidation of Copper. I. Physical Mechanism1a, JACS, 72 (1950) 5102-5106.
[66] Y.M. Shul'ga, V.I. Rubtsov, V.N. Vasilets, A.S. Lobach, N.G. Spitsyna, E.B. Yagubskii, EELS, XPS and IR study of $C_{60} \cdot 2S_8$ compound, Synth. Met., 70 (1995) 1381-1382.
[67] D. Bahrin, Subagjo, H. Susanto, Effect of Regeneration Temperature onParticle Characteristics and Extent of Regeneration of Saturated SO_2-Adsorption of $CuO/\gamma\text{-}Al_2O_3$ Adsorbent, Procedia Chem., 16 (2015) 723-727.
[68] S.-F. Cheah, G.E. Brown, G.A. Parks, XAFS Spectroscopy Study of Cu(II) Sorption on Amorphous SiO_2 and $\gamma\text{-}Al_2O_3$: Effect of Substrate and Time on Sorption Complexes, JCIS, 208 (1998) 110-128.
[69] S.-F. Cheah, G.E. Brown, Jr., G.A. Parks, XAFS study of Cu model compounds and Cu^{2+} sorption products on amorphous SiO_2, $\gamma\text{-}Al_2O_3$, and anatase, AmMin, 85 (2000) 118-132.
[70] W.H. Cassinelli, L. Martins, A.R. Passos, S.H. Pulcinelli, A. Rochet, V. Briois, C.V. Santilli, Correlation between Structural and Catalytic Properties of Copper Supported on Porous Alumina for the Ethanol Dehydrogenation Reaction, ChemCatChem, 7 (2015) 1668-1677.

[71] X. Meng, H. Pan, T. Zhong, X. Zhang, Unique chemoselective Mukaiyama aldol reaction of silyl enol diazoacetate with aldehydes and acetals catalyzed by MgI2 etherate, Tetrahedron, 75 (2019) 130682.
[72] G. Hao, R. Zhang, J. Li, B. Wang, Q. Zhao, Insight into the effect of surface structure on H_2 adsorption and activation over different CuO(111) surfaces: A first-principle study, Comput. Mater. Sci., 122 (2016) 191-200.
[73] J.Y. Kim, J.A. Rodriguez, J.C. Hanson, A.I. Frenkel, P.L. Lee, Reduction of CuO and Cu_2O with H_2: H Embedding and Kinetic Effects in the Formation of Suboxides, JACS, 125 (2003) 10684-10692.
[74] J.A. Rodriguez, J. Hrbek, Interaction of Sulfur with Well-Defined Metal and Oxide Surfaces: Unraveling the Mysteries behind Catalyst Poisoning and Desulfurization, Acc. Chem. Res., 32 (1999) 719-728.
[75] N. İnoğlu, J.R. Kitchin, Sulphur poisoning of water-gas shift catalysts: site blocking and electronic structure modification, Mol. Simul., 35 (2009) 936-941.
[76] P. Kratzer, B. Hammer, J.K. Nørskov, Geometric and electronic factors determining the differences in reactivity of H_2 on Cu(100) and Cu(111), Surf. Sci., 359 (1996) 45-53.
[77] B. Hammer, M. Scheffler, K.W. Jacobsen, J.K. Nørskov, Multidimensional Potential Energy Surface for H_2 Dissociation over Cu(111), Phys. Rev. Lett., 73 (1994) 1400-1403.
[78] C.S. Alexander, J. Pritchard, Chemisorption of hydrogen on evaporated copper films, J. Chem. Soc., Faraday Trans. 1, 68 (1972) 202-215.
[79] M. Cacciatore, G.D. Billing, Dissociation and atom recombination of H_2 and D_2 on metallic surfaces: A theoretical survey, Pure Appl. Chem., 68 (1996) 1075-1081.
[80] P.D. Vaidya, V.V. Mahajani, Kinetics of Liquid-Phase Hydrogenation of Furfuraldehyde to Furfuryl Alcohol over a Pt/C Catalyst, Ind. Eng. Chem. Res., 42 (2003) 3881-3885.
[81] A.B. Merlo, V. Vetere, J.F. Ruggera, M.L. Casella, Bimetallic PtSn catalyst for the selective hydrogenation of furfural to furfuryl alcohol in liquid-phase, Catal. Commun., 10 (2009) 1665-1669.
[82] P. Mäki-Arvela, L.-P. Tiainen, A.K. Neyestanaki, R. Sjöholm, T.-K. Rantakylä, E. Laine, T. Salmi, D.Y. Murzin, Liquid phase hydrogenation of citral: suppression of side reactions, Appl. Catal., A, 237 (2002) 181-200.
[83] P.G.N. Mertens, F. Cuypers, P. Vandezande, X. Ye, F. Verpoort, I.F.J. Vankelecom, D.E. De Vos, Ag^0 and Co^0 nanocolloids as recyclable quasihomogeneous metal catalysts for the hydrogenation of α,β-unsaturated aldehydes to allylic alcohol fragrances, Appl. Catal., A, 325 (2007) 130-139.
[84] F.A.J. Meskens, Methods for the Preparation of Acetals from Alcohols or Oxiranes and Carbonyl Compounds, Synthesis, 1981 (1981) 501-522.
[85] R. Kumar, A.K. Chakraborti, Copper(II) tetrafluoroborate as a novel and highly efficient catalyst for acetal formation, Tetrahedron Lett., 46 (2005) 8319-8323.
[86] J.-H. Lin, C.-S. Chen, H.-L. Ma, C.-Y. Hsu, H.-W. Chen, Synthesis of MWCNTs on $CuSO_4/Al_2O_3$ using chemical vapor deposition from methane, Carbon, 45 (2007) 223-225.
[87] V.V. Pushkarev, N. Musselwhite, K. An, S. Alayoglu, G.A. Somorjai, High Structure Sensitivity of Vapor-Phase Furfural Decarbonylation/Hydrogenation Reaction Network as a Function of Size and Shape of Pt Nanoparticles, Nano Lett., 12 (2012) 5196-5201.